Monte-Carlo simulation of a slot-scanning X-ray imaging system

Mayuresh Kulkarni*, Ronald Dendere*, Fred Nicolls†, Stef Steiner*^, Tania S. Douglas*[1]

*Division of Biomedical Engineering, University of Cape Town
^Lodox Systems, Sandton, Johannesburg
†Department of Electrical Engineering, University of Cape Town

[1]corresponding author

Abstract

We present a method for simulating slot-scanning X-ray imaging using the general-purpose Monte Carlo simulation package PENELOPE and penEasy Imaging. Different phantoms can be defined with the PENGEOM package, which defines bodies as combinations of volumes limited by quadric surfaces. The source-detector geometry, the position of the object, the collimator, the X-ray tube properties, the detector material and the pixel dimensions are defined. The output of the time-delay integration detector is simulated using sequential slot outputs derived from penEasy Imaging. The simulations are validated using tungsten and aluminium test objects, which are both simulated and imaged. The simulations are compared to the X-ray images using standard image quality metrics. The MTF, NPS and DQE curves show that the real and simulated X-ray images are comparable in terms of spatial resolution, noise and frequency information. The implementation can be modified to suit alterations in the system being simulated.

Keywords

Monte-Carlo, simulation, slot-scanning, X-ray

I. Introduction

Several models have been developed to simulate the design and optimisation of X-ray imaging systems, but they either only simulate parts of the imaging chain like the X-ray energy spectrum [1] and scattered radiation [2], or are not sufficiently flexible to simulate different phantoms and imaging systems [3], [4]. Furthermore, few simulation methods are available for slot-scanning imaging, and those that exist are application-specific and limited in their use. This paper describes a flexible and multi-purpose simulation tool for slot-scanning digital X-ray imaging using Monte-Carlo methods for radiation transfer with a flexible geometric setup.

II. Background

X-ray simulation tracks the path of X-ray photons from the source, through the test object to the detector, and is essentially a radiation transport problem. The Boltzmann equation was initially used to study radiation transport problems, but had considerable limitations for simple geometries [5]. In the early 1960s, with computing advances, Monte-Carlo (MC) simulations emerged as a powerful tool for radiation transport problems. Several MC implementations are available, such as ITS3 [6], EGS4 [7], EGS5 [8], GEANT3 [9], GEANT4 [10] and others.

XRaySim [3] is an open-source simulation package for industrial non-destructive testing and medical imaging applications. It uses C++ and open-source libraries to simulate X-rays. The input energy spectra are simulated using standard MC methods, while phantoms and their material properties are used to acquire simulated X-ray images on specified detectors. Phantom geometry can be modified using commercial CAD packages, custom materials can be defined and defects in test objects can be simulated. Detector characteristics can be defined and various scan geometries can be simulated. XRaySim does not support slot-scanning X-ray imaging and is not able to do high-resolution simulations (e.g. 50microns/pixel).

The work done in [4] explains a simulation setup similar to XRaySim based on triangular mesh geometry, radiation transfer and ray-tracing, used with the X-ray attenuation law to simulate 3D phantoms for non-destructive testing (NDT). The imaging process comprises defining X-ray source, beam, test object and detector. The work has potential applications beyond NDT, but development is in the early stages and the code is not publicly available. The simulation does not currently have the flexibility for extension to slot-scanning X-ray imaging systems.

Hussein et al. [11] simulated a tissue-equivalent breast phantom image and compared it to X-ray images from a slot-scanning mammography system. The simulations were based on source models as well as empirical equations for pixel intensities, scattered radiation and other variables in the imaging chain. The simulated images were validated by comparison to real X-ray images of the phantom, using image contrast, contrast-to-noise ratio, noise power spectrum, modulation transfer function and detective quantum efficiency. The simulated images were found to be comparable to the real images. Monte-Carlo methods and ray-tracing were not used. A limitation of this work is that it simulates the mammography imaging setup with one specific phantom and does not lend itself to modelling different phantoms, materials, geometries or X-ray sources.

III. Slot-scanning simulation methodology

This section describes the components of a generic X-ray imaging system and their simulation using PENELOPE and penEasy Imaging.

A. PENELOPE and penEasy Imaging

A typical MC X-ray implementation consists of modelling the physics of the imaging process and tracking the geometry of the rays. PENetration and Energy LOss of Positrons and Electrons (PENELOPE) [5], developed by the Nuclear Energy Agency (NEA), is a set of Fortran subroutines that model the transport of photons through different media. The interaction between media and radiation, in the energy range from 50eV to 1 GeV, is simulated. PenGEOM defines the geometry of the system using either voxel geometry or quadrics. The RITA (Rational Inverse Transform with Aliasing) algorithm is used to simulate coherent and incoherent scattering of photons in PENELOPE.

PENELOPE and its various subroutines have been widely used to develop tools to simulate complex geometries and phantoms. The basic simulation of an X-ray image using PENELOPE is defined in penEasy Imaging [12]. General-purpose Monte-Carlo simulations of radiation transport using PENELOPE are combined with a flexible geometric setup based on triangular meshes in penMesh [13]. These were used to define anthropomorphic phantoms to simulate X-ray images in [14]. The tools have been used to generate clinically-realistic projection images and computed tomography scans of the Duke phantom of the human body [15].

B. X-ray source and Collimation

A 90kV-100mA rectangular beam source, also known as a fan-beam, is defined using penEasy Imaging. It provides a collimated beam, beam width 6mm, of radiation that produces a rectangular radiation field on the detector, to resemble a cone beam emitted from a point focal spot; the beam is collimated using lead as an ideal collimator with total absorption and no scatter radiation. The source-to-detector distance is 1296mm, with an inherent 1mm aluminium filter. Variables like the polar and azimuthal apertures, the direction of the fan-beam and the source location in the overall geometry enable modification of the source to match the physical one. Different energy spectra may be used.

Post-collimation filters are frequently used to improve scatter or reduce X-ray dose. They can be modelled by altering the energy spectra. Adding the filter to the geometry, at the desired location and with the desired material properties, is another way of modelling filters. A filter of a specific thickness and material is incorporated into the simulation as a plane in the geometric system. Photon transport is followed through the filter to the detector.

C. Imaging Geometry

Figure 1 displays a typical slot scanning system, showing the effect of collimation and the relationship between collimator width and beam width. An image is formed as the source moves with respect to the detector in the scan direction, which is perpendicular to the slot direction.

The imaging geometry can be divided into two parts, namely the object geometry and the system geometry. The object geometry defines the shape and size of the object being scanned. PENGEOM splits an object into its quadric components (surfaces of varying 3D shapes) and assigns them material properties using the PENELOPE material database, which covers over 200 materials including elements, compounds and mixtures. The position of the object between the source and the detector forms part of the geometry.

The system geometry contains information about the locations of the source, the detector and the object. The apertures of the source and the source-detector distance determine the detector size to be used. The number of pixels on the detector, and hence the resolution, can be set.

The penEasy Imaging package provides tools to obtain the X-ray image output from PENELOPE [12]. Thus PENELOPE handles the physics of photon travel, RITA provides scatter modelling, PENGEOM contains the geometrical information, and penEasy Imaging converts the detector signal into output. The system geometry shown in Figure 1 is defined using the PENGEOM package.

D. TDI detector

The time delay integration (TDI) read-out technique, also known as drift scanning, divides the detector into columns or slots representing the collimated beam. The distance between two slots can be defined. The slots generally overlap to ensure that a certain area on the detector occurs in many slots. Combining the slots averages the output at the detector, reducing the noise and scattered radiation. Over the period of a scan, each slot is exposed to X-rays and is clocked out of the detector. All the individual scans are integrated to produce the final X-ray image. Figure 2 shows two consecutive slots in the detector.

The step is the distance between the beginnings of consecutive slots. The step width can be set for simulation. A larger step size reduces the run time.

E. Image acquisition and simulation

This work uses the subroutines in PENELOPE to model the Lodox Statscan (Sandton, South Africa) slot-scanning X-ray system. The basic implementation has been modified to perform iterative slot scanning, by dividing the detector into many slots, obtaining the exposures at each slot and integrating all the slots on the detector to produce the final image. The simulations assume "no lag" i.e. that there is no correlation in image data between successive positions of the slot during the scan.

A 90kV-100mA X-ray source with a narrow focal spot (0.5mm) is used for simulations and its energy spectrum, shown in Figure 3, is defined using Spekcalc [1]. The total current-time product (300mAs) and aluminium first half value layer (2.11mm) for the simulations is the same as used for a Lodox scan, to ensure a match in the average radiation exposure. Filtration parameters, such as material and thickness, as well as tube output parameters, are set in SpekCalc to match those of the Lodox system. The number of photon histories was determined using the X-ray tube current and charge per X-ray photon, to match that of the system. Spekcalc is used to simulate the energy spectrum from specific anodes and filters that match the Lodox X-ray source. Collimation, photon transfer effects and X-ray beam formation are controlled using the simulation geometry. The detector is a 10cm-by-10cm CsI layer of thickness 0.6mm. The angles of the fan beam and the collimator width were set to cover a 10cm, 2000-pixel detector, with each slot having a beam width of 1mm. The step between slots was 1 pixel. The resolution of the detector was set to 50 microns, to approximately match the resolution of the Lodox Statscan machine. The scintillator and its noise characteristics are modelled to ensure that the real and simulated X-ray images are similarly acquired. The electronic (system) noise was not modelled since it is machine-dependent. The Lodox Statscan system uses binning of pixels, usually 5x5 binning, to reduce image granularity. Pixel binning was not simulated as it is an operation performed after image acquisition. However, binning was performed on the simulated data using localized median filters to match the binning levels of the imaging system. Two simple test objects were used to evaluate the simulations. A 2mm thick tungsten object was imaged using the Lodox StatScan and simulated using the same parameters. An aluminium object containing 5 aluminium blocks of different thicknesses was simulated and imaged. The aluminium blocks were chosen to study the contrast at different thicknesses. In the X-ray and the simulated images, four non-overlapping regions in the background were selected. The image contrast and CNR were calculated for four corresponding regions in the real and simulated X-ray images and compared. The tungsten object was used to obtain a sharp edge to calculate the edge spread function, and subsquently the

MTF and the DQE. The tungsten block was placed at an angle of 2 degrees to the scan direction as described in [16]. The simulations were performed using a cluster of computers at the High Performance Computing Center at the University of Cape Town, where slots were simulated in parallel to speed up the simulation process.

F. Image quality

Image contrast, contrast-to-noise ratio and photon noise have been discussed in the context of comparing X-ray images to simulations [17]. If $S_{background}$ and S_{ROI} are mean intensities of the background and regions of interest (ROI), respectively, image contrast is defined as:

$$C_{img} = \frac{S_{background} - S_{ROI}}{S_{background}} \quad (1)$$

and the contrast-to-noise ratio is:

$$CNR_{img} = \frac{S_{ROI} - S_{background}}{noise} \quad (2)$$

The noise was assumed to be the result of quantum noise, dark noise, electronic and digitization noise. The standard deviation of pixel values from the mean, of a uniform area in the background, was measured as noise.

A more detailed and objective assessment of X-ray images is discussed in [17], using three broad parameter types. The objective assessment can be used to compare images from different imaging systems, geometries and machines. The parameter types are a macro (over a large area) system transfer function, measures of spatial resolution and a measure of noise. The macro system transfer function is a relationship between the input X-ray quanta, and the output optical density. Measures of spatial resolution are the response of the system to small features, for example the blurring and displacement of the input signal. Generally the imaging system is considered as a linear and time invariant system and the measures of spatial frequency are the edge spread and the line spread functions. The modulation transfer function (MTF) is described as the frequency response of the line spread function. The final measure to analyse the image quality is the noise measure. Noise is measured in terms of the spatial frequency content, known as the noise power spectrum (NPS). The detective quantum efficiency (DQE) is the combination of all three measures.

The resolution properties of an image are defined by the MTF. The MTF is dependent on the edge spread function (ESF) and the line spread function (LSF) which are based on the sharpness of an edge in the image. Specifically, the MTF of a radiographic system can be determined by evaluating the response of the system to periodic patterns or by calculating the line spread function using a narrow slit formation [18], [19]. In this paper, the sharp edge method of calculating the LSF using the ESF [18] is used. The same method has been used previously to calculate the MTF on the Lodox Statscan slot-scanning system [16].

The DQE is defined as [20]:

$$DQE(v) = \frac{(S/N)^2_{out}(v)}{(S/N)^2_{in}(v)} \quad (3)$$

where S is the signal amplitude, N the noise power spectrum and v the spatial frequency. The spatial frequency is a vector in the case of X-ray images. There is some ambiguity with respect to the definition of the input signal and noise in the literature [22]. Most authors consider detectors as energy integrating devices so the energy is the relevant quantity.

This paper follows [16] which extends the definition of MTF and DQE for slot-scanning imaging systems. The basic formulation of the DQE based on [16], [20], [21] is:

$$DQE(v_x, v_y) = G^2 MTF^2 \frac{W_{in}^2(v_x,v_y)}{W_{out}^2(v_x,v_y)} \qquad (4)$$

where

- (v_x, v_y) = spatial frequency coordinates
- $W_{in}^2(v_x, v_y)$ = input noise power spectrum
- $W_{out}^2(v_x, v_y)$ = output noise power spectrum
- G = incremental gain used in converting pixel raw data to photon count
- MTF = modulation transfer function.

IV. Results and Discussion

The real and simulated X-ray images for the aluminium and tungsten test objects are shown in Figures 4a and 4b, respectively. A typical simulation time for a 10cm, 2000-pixel detector, with a slot width of 1mm and a step between slots of 1 pixel, was approximately 2 hours. This corresponds to 1000 slots and a detector resolution of 50 microns/pixel.

The image contrast and CNR for the real and the simulated X-ray images are compared in Figures 5a and 5b. The CNR depends on pixel intensity and noise; a difference of approximately 20% between measured and simulated CNR is acceptable [22]. The results discussed in [11] were obtained by estimating pixel values of the output X-ray image and comparing them to real X-rays using image contrast and CNR. The image contrast and CNR results in this paper are in agreement with [17]; the contrast and CNR values for real and simulated X-ray images overlap as shown in Figures 5b and 5a. The simulations in Figure 4a and 4b have greater granularity than the real images despite the application of binning using the localized filters. This is due to the fact that, in addition to pixel binning, the Lodox system automatically applies a smoothing filter to output images.

The MTF curves for the real and simulated x-ray images, shown in Figure 6a, are high for low frequencies and have a similar fall-off. The MTF curves are normalised between 0 and 1, so that MTF(0) = 1, i.e., the zero-frequency is set to 1 [16], [18]. The similarity in the MTF curves shows that the spatial resolution of the real X-ray image is being correctly modelled in the simulated image. The magnitude of the NPS and curve shape for the simulated image is similar to that of the real image and the fall-off is also consistent, as shown in Figure 6b, indicating that the nature of the noise is modelled correctly. The DQE curves of the real and simulated X-rays, shown in Figure 7, are based on the MTF and the NPS curves. The shape (slope of the fall-off and the frequency of the peak) of the DQE curves for the real and simulated X-ray images are similar. The MTF, NPS and DQE curves for the slot direction are significantly similar to the curves in the scan direction for the Lodox X-ray imaging system [16], [23], therefore, curves are only shown for the scan direction.

In improving any X-ray imaging system, it is useful to study how each variable in the imaging chain affects the X-ray image [19]. If the effect of each variable is known, the variables can be optimised to improve the output X-ray image. The simulation method described in this paper can be used to understand the effect of different variables like X-ray anode and cathode materials, collimator width, material and thickness of the test object and the material and physical properties of the detector. The PENGEOM geometry package also gives a flexible framework to explore variables such as source-to-detector distances, source-to-object distances, source-to-collimator distances, slot and beam widths and the step size between slots. These features make the simulation tool useful not only to study existing X-ray imaging systems but also to design new ones.

I. Conclusion

This paper has described a general and flexible simulation method for slot-scanning X-ray imaging, which can be used to simulate different phantoms, materials and imaging systems.

Acknowledgment

The authors thank Andreu Badal-Soler and Josep Sempau for assistance with PENELOPE. Funding was provided by Lodox Systems, CapeRay Medical, the South African National Research Foundation (NRF) and the Cancer Association of South African (CANSA).

REFERENCES

[1] Poludniowski G, Landry G, DeBlois F, Evans PM, Verhaegen F. SpekCalc: a program to calculate photon spectra from tungsten anode X-ray tubes. Phys. Med. Biol. 2009; 54:433-8.

[2] Boone JM, Lindfors KK, Cooper NII, Seibert JA. Scatter/primary in mammography: Comprehensive results. Medical Physics. 2000; 27:2408- 2416.

[3] Viswanathan K, Balasubramaniam K. Modeling and simulation schemes in X-ray radiography and Computed Tomography, Proceedings of the National Seminar and exhibition on Non- Destructive Evaluation NDE 2009, Trichy, India. 2009.

[4] Freud N, Duvauchelle P, Babot D. Simulation of X-ray NDT imaging techniques. Proceedings of the 15th World Conference on Non-Destructive Testing. 2000; 15.

[5] Salvat F, Fernandez-Varea JM, Sempau J. PENELOPE-2008: A Code System for Monte Carlo Simulation of Electron and Photon Transport, Issy-les-Moulineaux, France: OECD Nuclear Energy Agency 2009. Available at http://www.nea.fr.

[6] Halbleib JA, Kensek RP, Mehlhorn TA, Valdez GD, Seltzer SM, Berger MJ. ITS version 3.0: the integrated TIGER series of coupled electron/photon Monte Carlo transport codes, Report SAND91-1634 (Sandia National Laboratories, Albuquerque, NM), 1992.

[7] Nelson WR, Hirayama H, Rogers DWO. The EGS4 Code System, Report SLAC-265 (Stanford Linear Accelerator Center, Stanford, CA), 1985.

[8] Hirayama H, Namito Y, Bielajew AF, Wilderman SJ, Nelson WR. The EGS5 Code System, SLAC-R-730 and KEK Report 2005-8 (Stanford Linear Accelerator Center, Stanford, CA), 2005.

[9] Brun R, Bruyant F, Maire F, McPherson AC, Zanarini P. GEANT3, Report DD/EE/841 (CERN, Geneva). 1986.

[10] Agostinelli S, Allison J, Amako K, Apostolakis J, Araujo H, Arce P et al. Geant4a simulation toolkit, Nucl. Instrum. Meth. A. 2003; 506:250-303.

[11] Hussein K, Vaughan CL, Douglas TS. Modelling, validation and application of a mathematical tissue-equivalent breast phantom for linear slot-scanning digital mammography. Physics in Medicine and Biology. 2009; 54:1533-1553.

[12] Badal-Soler A. Development of advanced geometric models and acceleration techniques for Monte Carlo simulation in Medical Physics. PhD Thesis, Universitat Polite`cnica de Catalunya. 2008.

[13] Badal A, Kyprianou I, Banh DP, Badano A, Sempau J. penMesh Monte Carlo radiation transport simulation in a triangle mesh geometry. IEEE Trans Med Imaging. 2009; 28(12):1894-901.

[14] Badal A, Kyprianou IS, Badano A, Sempau J, Myers KJ. Monte Carlo package for simulating radiographic images of realistic anthropomorphic phantoms described by triangle meshes. SPIE Medical Imaging: Physics of Medical Imaging. 2007. Proc. SPIE 6510.

[15] Badal A, Badano A. Accelerating Monte Carlo simulations of photon transport in a voxelized geometry using a massively parallel Graphics Processing Unit. Medical Physics. 2009; 36:4878-4880.

[16] De Villiers M, De Jager M. Detective Quantum Efficiency of the LODOX System, Proc. of SPIE, Vol. 5030, Medical Imaging, 2003.

[17] International Commission on Radiation Units and Measurements ICRU. Medical Imaging - the assessment of image quality, ICRU Report 54, 1996.

[18] Samei E, Flynn MJ, Reimann DA. A method for measuring the pre-sampled MTF of digital radiographic systems using an edge test device. Medical Physics. 1998; 25:102-113.

[19] Martin C, Sharp P, Sutton D. Measurement of image quality in diagnostic radiology. Applied Radiation and Isotopes. 1999; 50(1): 21-30.

[20] Stierstorfer K, Spahn M. Self-normalizing method to measure the detective quantum efficiency of a wide range of X-ray detectors. Medical Physics. 1999; 26:1312-1318.

[21] IEC 62220-1 Medical electrical equipment - Characteristics of digital X-ray imaging devices - Part 1: Determination of detective quantum efficiency.

[22] Doyle P, Martin CJ, Gentle D. Application of contrast-to-noise ratio in optimizing beam quality for digital chest radiography: comparison of experimental measurements and theoretical simulations. Physics in Medicine and Biology. 2006; 51:2953-2970.

[23] Scheelke M, Potgieter JH, de Villiers M. System characyerization of the STATSCAN full body slit scanning radiography machine: Theory and experiment. SPIE Medical Imaging: Physics of Medical Imaging. 2005. Proc. SPIE 5745.

FIGURE CAPTIONS

Fig. 1: Typical slot scanning X-ray system. SDD: source-to-detector distance, CDD: collimator to detector distance, x: thickness of the object to be scanned, Cw: collimator width, Bw: beam-width at the detector. The slot direction is coming out of the page and the scan direction is from left to right.

Fig. 2: TDI detector operation, two consecutive slots shown in top view and front view. The beam-width Bw is also the width of the slot. The step is the space between the beginnings of two slots. The detector output is an integration of the slots. The beam width and the step are shown in the top and front view.

Fig. 3: The tungsten energy spectrum at a distance of 1296mm for tube voltage of 90kVp, 100mA and aluminium filtration of 1mm computed using SpekCalc.

Fig. 4: The simulated (top) and real (bottom) images of the (a) aluminium and (b) tungsten test objects. The tungsten test object is at a slight angle to the detector for the DQE calculation.

Fig. 5: (a) Image contrast and (b) contrast-to-noise ratio for four different, non-overlapping regions of the background for corresponding locations in real (circles) and simulated (squares) images of the aluminium test object.

Fig. 6: (a) MTF and (b) NPS (log scale) of the real (continuous line) and simulated (dashed line) X-ray images. The x-axis of the NPS plot has been truncated at 1 lp/mm to highlight the fall-off points of the two curves.

Fig. 7: The DQE of the real (continuous line) and simulated (dashed line) images.

Figure

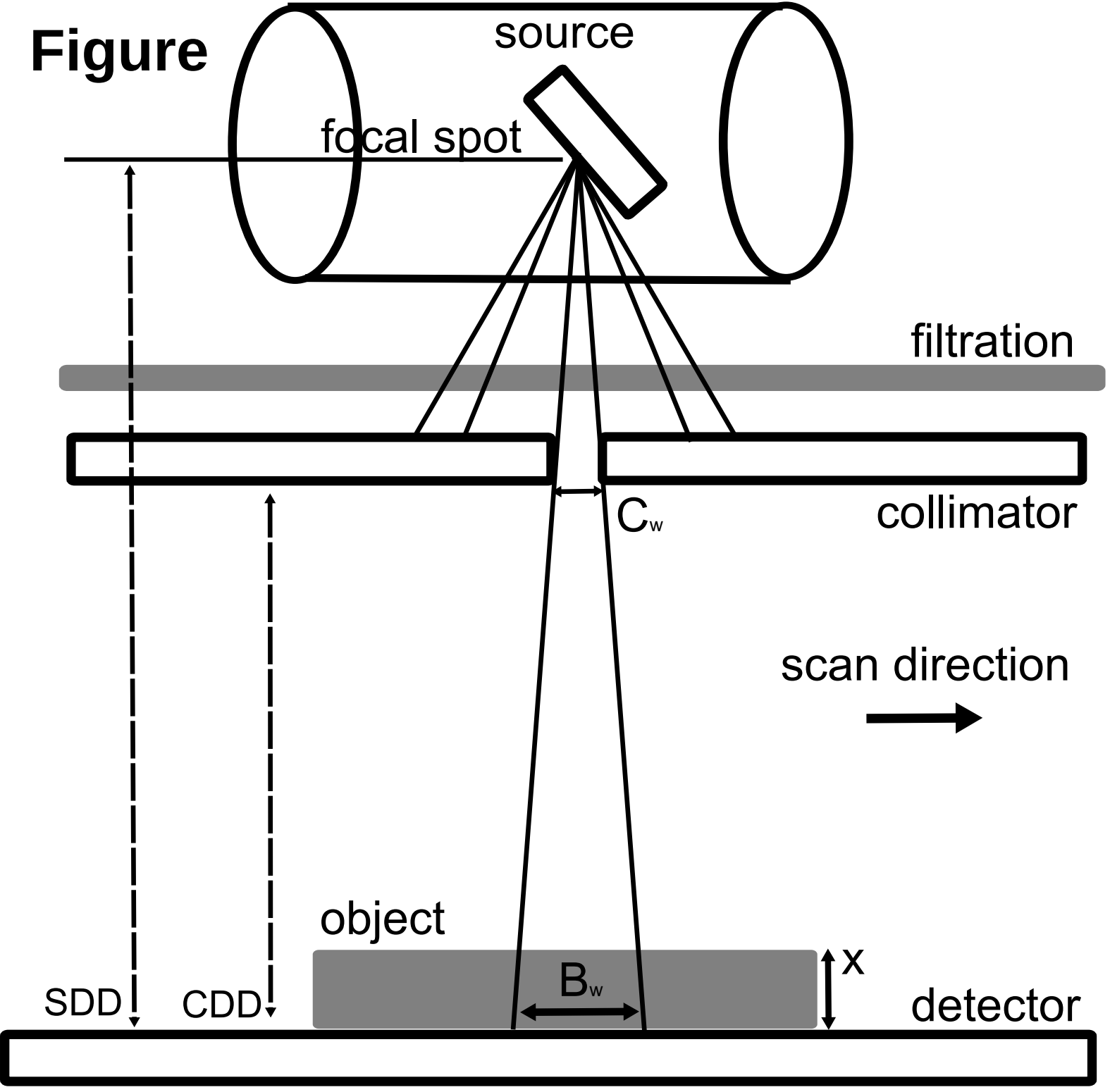
source
focal spot
filtration
collimator
C_w
scan direction
object
B_w
x
SDD
CDD
detector

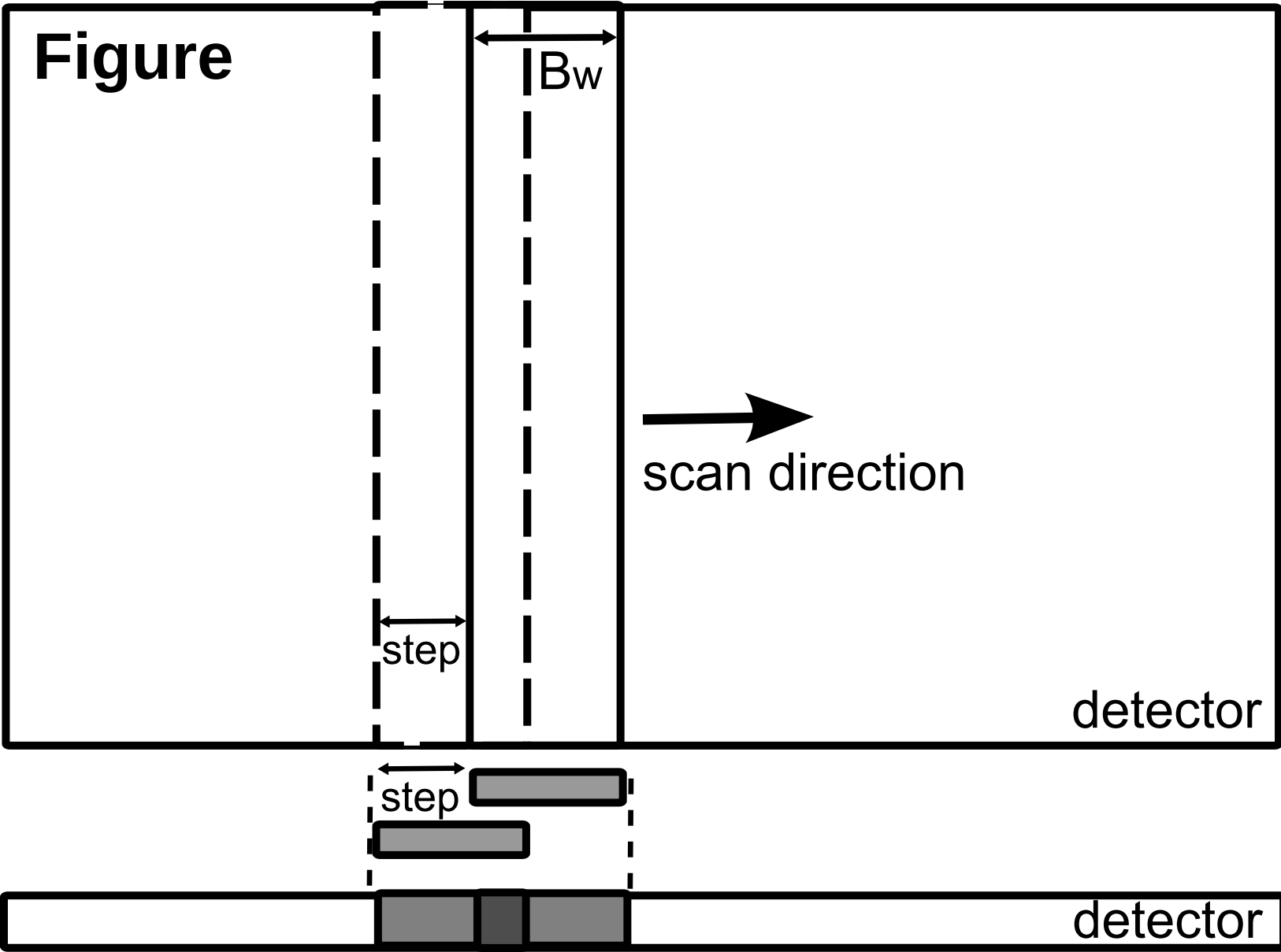
Figure
Bw
scan direction
step
detector
step
detector

Figure

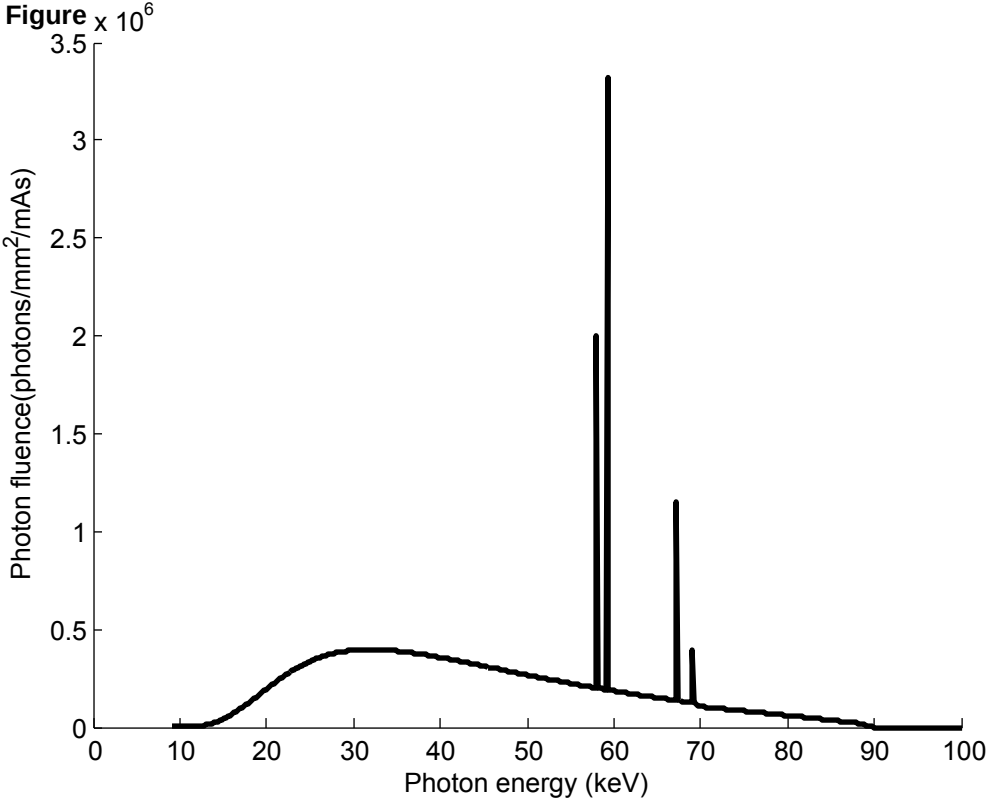
x 10^6
3.5
3
2.5
2
1.5
1
0.5
0
Photon fluence(photons/mm^2/mAs)
0
10
20
30
40
50
60
70
80
90
100
Photon energy (keV)

Figure

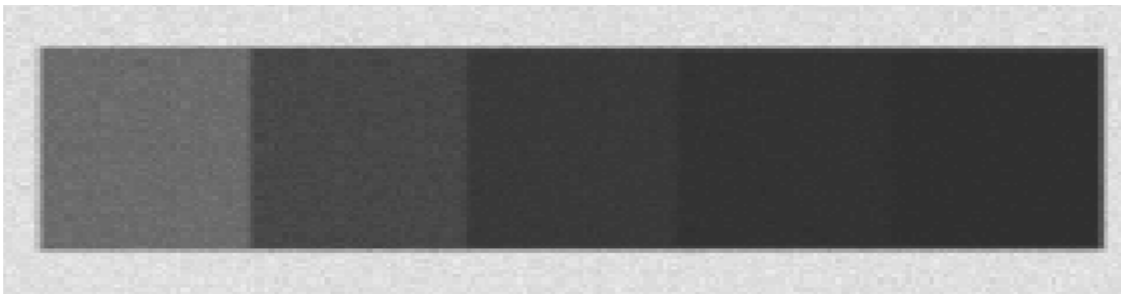

Figure

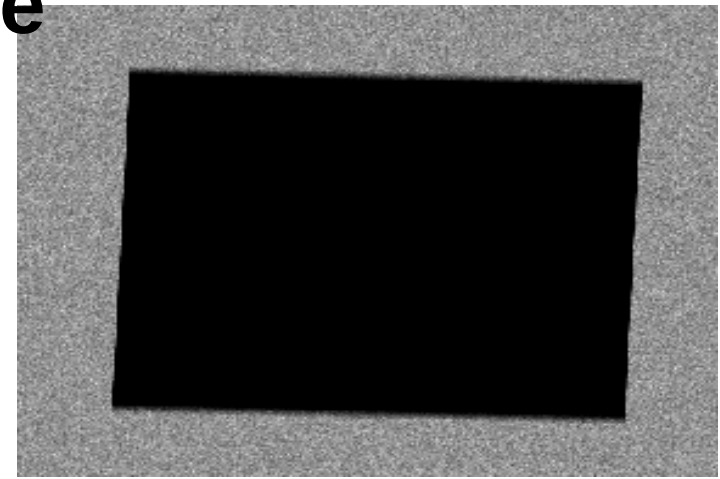

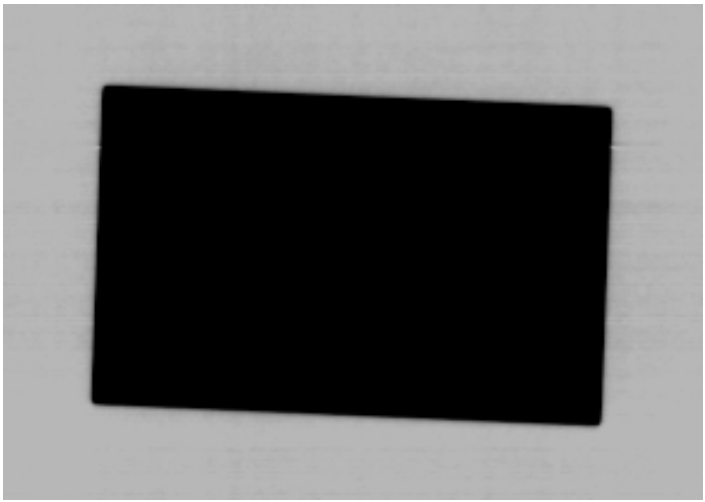

Figure

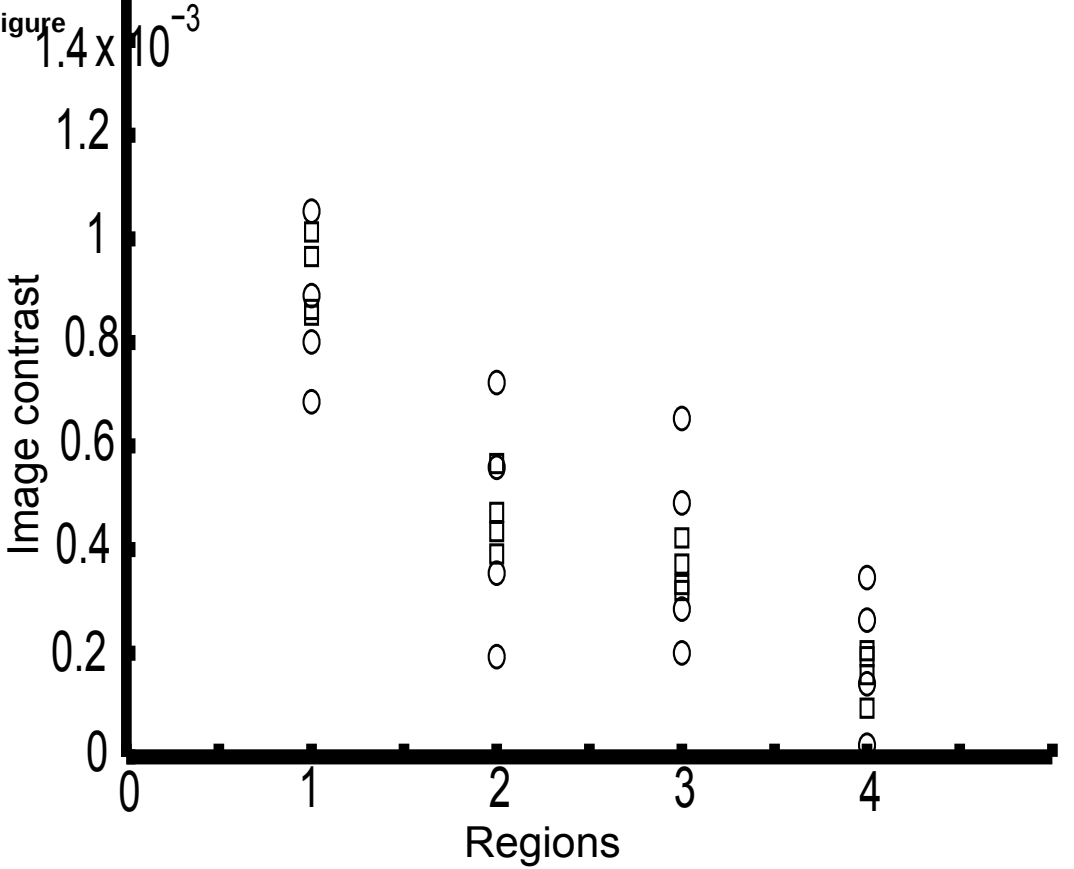

Figure

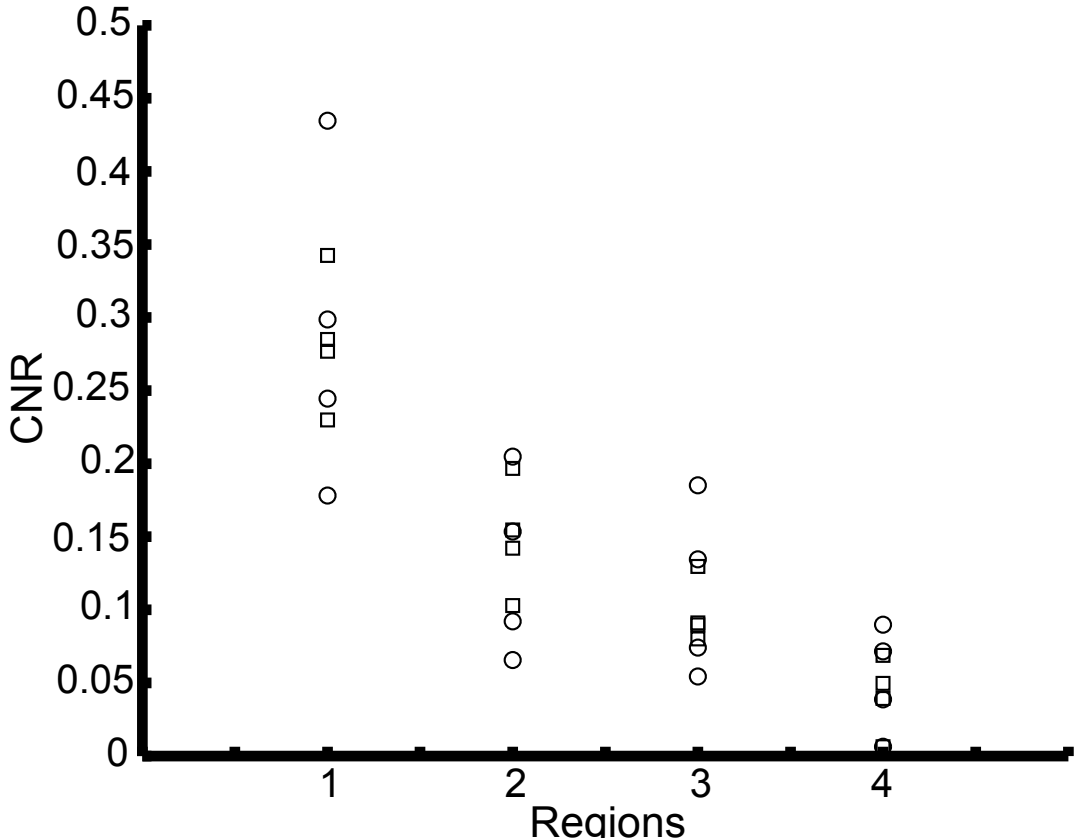

Figure

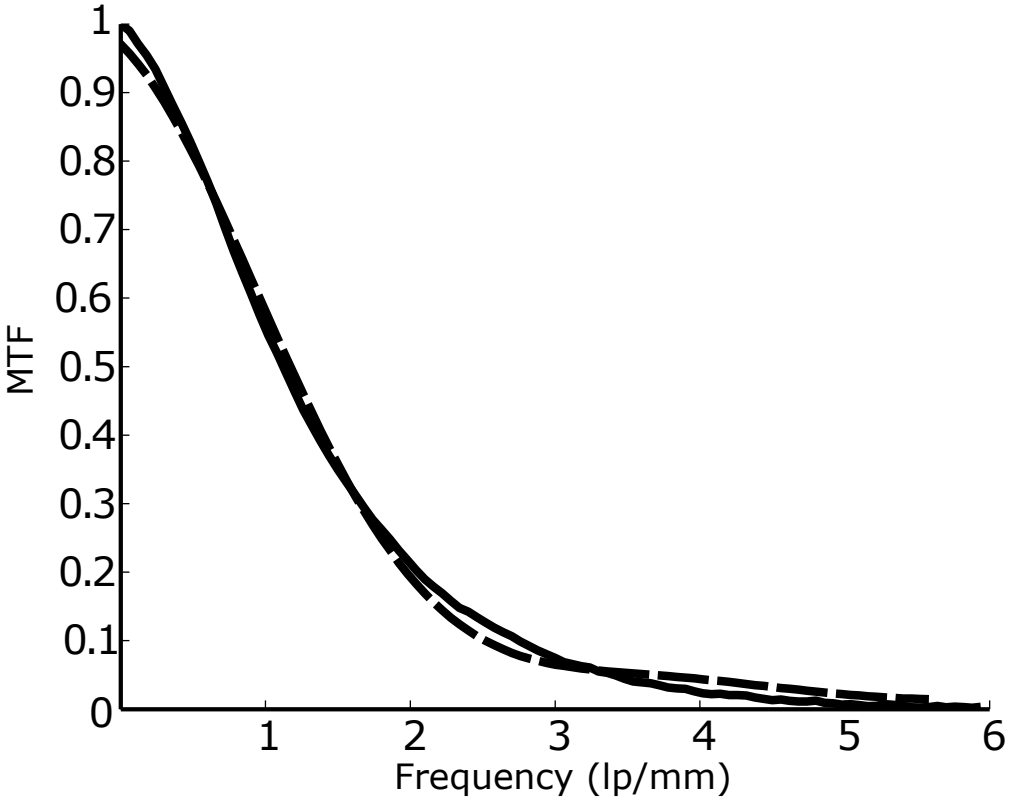

Figure

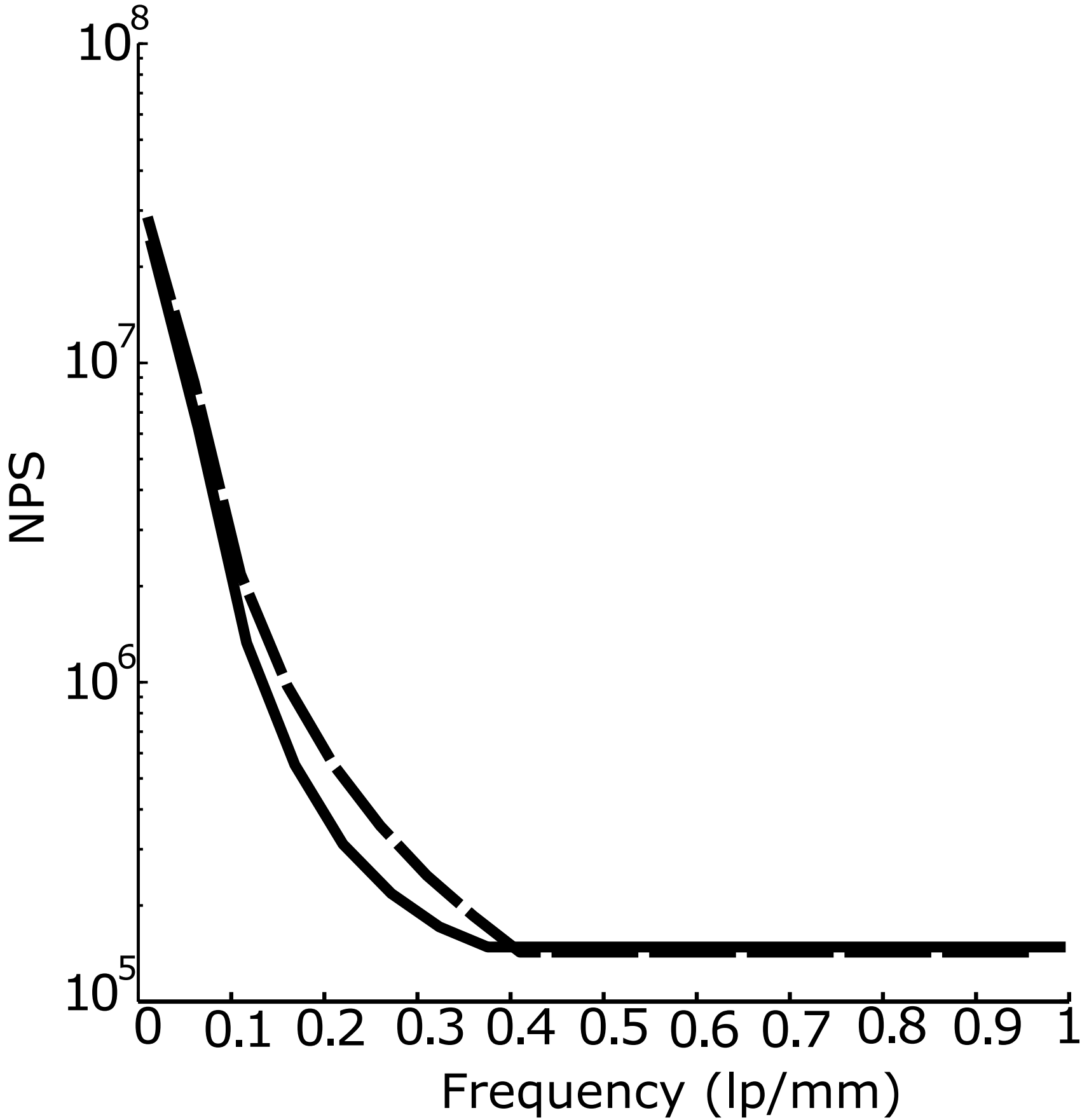

Figure